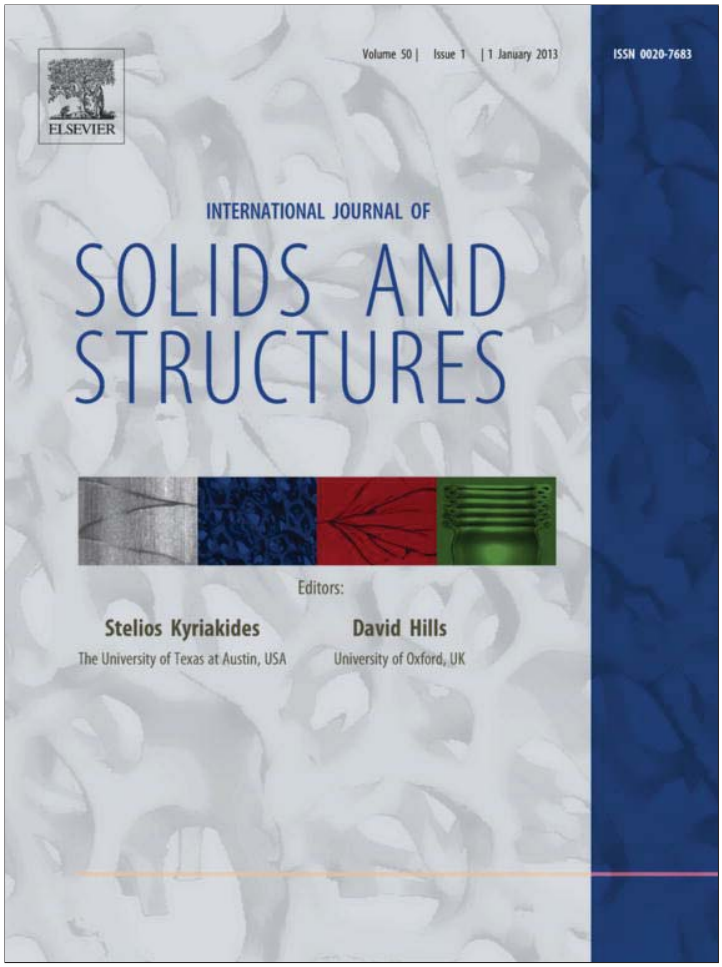

International Journal of Solids and Structures 50 (2013) 1–14

Contents lists available at SciVerse ScienceDirect

International Journal of Solids and Structures

journal homepage: www.elsevier.com/locate/ijsolstr

Circular loads on the surface of a half-space: Displacement and stress discontinuities under the load

Vlado A. Lubarda *

Department of Mechanical and Aerospace Engineering, University of California, San Diego, La Jolla, CA 92093-0411, USA
Montenegrin Academy of Sciences and Arts, Rista Stijovića 5, 81000 Podgorica, Montenegro

ARTICLE INFO

Article history:
Received 29 March 2012
Received in revised form 23 August 2012
Available online 15 September 2012

Keywords:
Discontinuities
Elasticity
Half-space
Radial shear
Ring load
Surface stresses

ABSTRACT

Based on the expressions for the surface displacements due to concentrated vertical and tangential forces acting on the free surface of a half-space, available from the well-known Boussinesq and Cerruti elasticity problems, the surface displacements and the surface stresses are derived for a half-space loaded by the vertical and tangential circular ring loads, or by uniform normal and radial shear stresses applied within a circular or annular circular domains. By using different routes of integration, alternative forms of displacement expressions are derived from the concentrated force results. Betti's reciprocal theorem is used to relate the displacements due to radial and vertical ring loads. The displacement and stress discontinuities under these loads, or along the boundaries of the circular domains within which the uniform stress is applied, are evaluated and discussed. The radial and circumferential components of stress are discontinuous under the load whenever the slope of the radial displacement is discontinuous under that load.

1. Introduction

The present work was motivated by recent studies devoted to the determination of the deformed shape of the surface of a soft substrate due to deposited liquid drop (Pericet-Camára et al., 2008; Yu and Zhao, 2009; Liu et al., 2009; Roman and Bico, 2010; Olives, 2010; Das et al., 2011; Jerison et al., 2011; Lubarda and Talke, 2011; Lubarda, 2012). If the solid substrate is sufficiently soft, the distributed capillary force along the triple contact line between the solid/liquid/vapor phase, resulting from the surface tensions and intermolecular interactions around the triple contact (Fig. 1), can give rise to appreciable uplifting of the surface of the substrate below the triple contact line. The formation of circular ridges can have significant effects on the functioning of MEMS and other micro/nano devices, lubrication of magnetic hard disks, molten solder spreading in electronic packaging, etc. (Carré et al., 1996). This was studied by using a linear elasticity theory by many researchers, with the early contributions by Lester (1961) and Rusanov (1975), followed by Fortes (1984), Shanahan (1988) and Kern and Muller (1992). The elastic response in this problem is characterized by the singularity of the vertical component of displacement below the capillary force, assumed to be distributed as a circular line load. The elasticity solution also predicts a discontinuous radial displacement under the vertical line load. To eliminate this singularity, one approach is to distribute the capillary force within a finite width, related to the actual thickness of the interface liquid/vapor layer and the molecular interactions between a liquid drop and a solid substrate. This thickness may vary from 1 nm for harder substrates to microns for softer rubber or gel substrates (Lester, 1961; Rusanov, 1975; de Gennes, 1985; Yu and Zhao, 2009), but is, in any case, much smaller than the radius R of the contact circle (Fig. 1). Even though such procedure eliminates the vertical displacement singularity, it does not eliminate the discontinuity in the slope of the radial displacement at the boundaries of the annular circular region within which the capillary force is distributed, and this gives rise to the discontinuity in both the radial and circumferential stresses across these boundaries. The effect of stress on the wetting angle was studied by Srolovitz and Davis (2001), who found that elastic effects in solids are incapable of modifying the wetting angle determined by interfacial tensions, except in crack-like geometries. Recently, Style and Dufresne (2012) examined the effect of the surface tension and the elastocapillary length on the peak displacement under the load. Marchand et al. (2012) determined the effective surface tension from the elastic displacement field of a thin elastomeric wire immersed in a liquid bath, observing experimentally an unexpected direction of the force transmission along the contact line.

The stress discontinuity also arises in the classical Love's (1929) problem of a semi-infinite solid loaded by a uniform pressure p within a circular area, in which the radial and circumferential stress discontinuities across the loading boundary are of magnitude p and

* Address: Department of Mechanical and Aerospace Engineering, University of California, San Diego, La Jolla, CA 92093-0411, USA. Tel.: +1 858 534 3169; fax: +1 858 534 5698.
E-mail address: vlubarda@ucsd.edu

0020-7683/$ - see front matter © 2012 Elsevier Ltd. All rights reserved.
http://dx.doi.org/10.1016/j.ijsolstr.2012.08.029

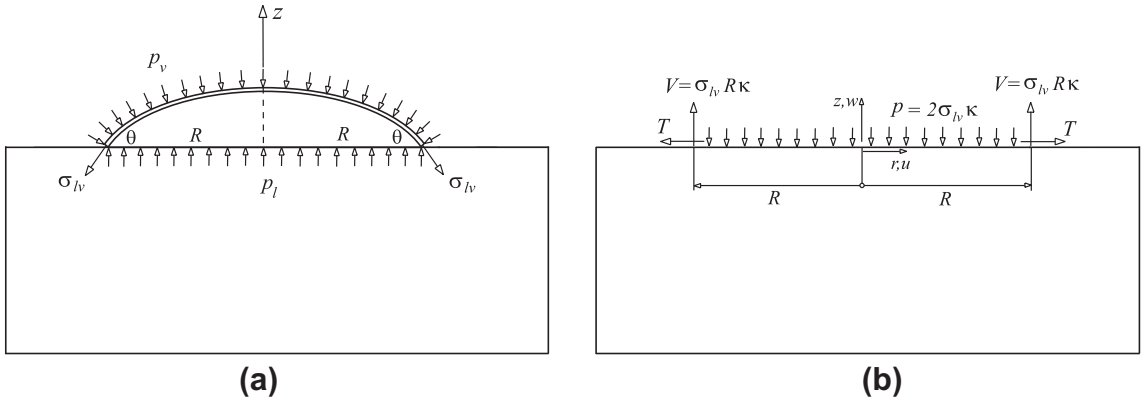

Fig. 1. (a) A free-body diagram of a liquid drop. The liquid pressure is p_l, the vapor pressure is p_v, and the liquid/vapor surface tension is σ_{lv}. (b) A self-equilibrated loading on the surface of the substrate, consisting of pressure $p = 2\kappa\sigma_{lv}$, vertical line force $V = \sigma_{lv}\sin\theta = R\kappa\sigma_{lv}$, and the tangential (radial) line force $T = \sigma_{lv}\cos\theta$, where θ is the Young's contact angle. The liquid/vapor surface tension is σ_{lv}. The mean curvature of the drop around the triple contact line of radius R is κ.

$2vp$, respectively. See also Sneddon (1951) discussion of Terezawa (1916) solution. In the case of uniform radial shear stress applied within the circle of radius R, the slope of the radial displacement becomes infinite at the center ($r = 0$) and along the boundary $r = R$, which results in the stress singularities at these points as well. If the shear stress is distributed within an annular region $R_0 \leqslant r \leqslant R$, the singularity at the center is eliminated, but the stresses are still singular along the circles $r = R_0$ and $r = R$. In the limit as $R_0 \to R$, the solution for the radial ring load is recovered, for which the radial displacement and its slope, and thus the radial and circumferential stresses, are all singular under the load, while the vertical displacement is finite but discontinuous.

The solutions for some of the elasticity problems considered in this paper have been previously constructed and reported in the literature, e.g., Sneddon (1951), Timoshenko and Goodier (1970) and Johnson (1985), or can be deduced from them by an appropriate integration, but the stress and displacement discontinuities, inherently imbedded in these solutions, were not fully discussed or examined. Furthermore, the expressions for the surface displacement and stress components for all loadings considered in this paper are derived by using the results for the surface displacements due to the concentrated vertical (Boussinesq) or tangential (Cerruti) force only, without resorting to involved solutions of the corresponding entire boundary value problems. Different expressions for the displacement components due to vertical and tangential ring loads are derived and discussed.

2. Surface displacement components due to concentrated force

For the later use in the paper, we list in this section the expressions for the surface displacements in the well-known Boussinesq and Cerruti concentrated force problems, and the surface displacements from the surface doublet and quadruplet acting on the boundary of an elastic half-space.

2.1. Boussinesq problem

In the Boussinesq elasticity problem, the displacement components of the points of the bounding surface ($z = 0$) of a half-space, due to the applied concentrated vertical force Q_z are given by (e.g., Johnson, 1985, p. 50)

$$u_\xi = \frac{Q_z(1-2\nu)}{4\pi G}\frac{\xi}{\rho^2}, \quad u_\eta = \frac{Q_z(1-2\nu)}{4\pi G}\frac{\eta}{\rho^2}, \quad u_z = \frac{Q_z(1-\nu)}{2\pi G}\frac{1}{\rho}, \tag{1}$$

where G is the elastic shear modulus and ν is the Poisson ratio. The in-plane Cartesian coordinates are (ξ, η) and ρ is the radial distance from the origin at which the force is applied. The radial displacement is accordingly

$$u_\rho = \frac{Q_z(1-2\nu)}{4\pi G}\frac{1}{\rho}. \tag{2}$$

The nonvanishing surface strain components are

$$\epsilon_\rho = \frac{\mathrm{d}u_\rho}{\mathrm{d}\rho} = -\frac{Q_z(1-\nu)}{2\pi G}\frac{1}{\rho^2}, \quad \epsilon_\theta = \frac{u_\rho}{\rho} = \frac{Q_z(1-\nu)}{2\pi G}\frac{1}{\rho^2} \equiv -\epsilon_\rho. \tag{3}$$

Since $\sigma_z = 0$ away from the load, the corresponding surface stress components are, from Hooke's law, $\sigma_\theta = -\sigma_\rho = 2G\epsilon_\theta$.

2.2. Cerruti problem

The displacement components due to the concentrated tangential force Q_ξ are (Cerruti problem; Johnson, 1985, p. 69)

$$u_\xi = \frac{Q_\xi}{2\pi G}\left(\frac{1}{\rho} - \nu\frac{\eta^2}{\rho^3}\right), \quad u_\eta = \frac{Q_\xi \nu}{2\pi G}\frac{\xi\eta}{\rho^3}, \quad u_z = -\frac{Q_\xi(1-2\nu)}{4\pi G}\frac{\xi}{\rho^2}. \tag{4}$$

The vertical displacement along the ξ-axis is singular and discontinuous at $\xi = 0$. The points $\xi > 0$ are depressed ($u_z < 0$), while the points $\xi < 0$ are elevated ($u_z > 0$). Note that $u_\xi^{-Q_z} = u_z^{Q_\xi}$, provided that the magnitude of the compressive force $(-Q_z)$ is equal to the magnitude of the shear Q_ξ; cf. (1) and (4). It is recalled that in a two-dimensional (plain-strain) version of the problem, the vertical displacement due to tangential concentrated force is finite but discontinuous under the force, $u_z = -Q_x(1-2\nu)\mathrm{sgn}(x)/(4G)$. Likewise, in a two-dimensional Flamant's problem, the horizontal displacement due to concentrated vertical force is $u_x = Q_z(1-2\nu)\,\mathrm{sgn}(x)/(4G)$.

2.3. Surface doublet

Two co-linear tangential forces Q at small distance d constitute a doublet of forces shown in Fig. 2(a). By superposition of results from (4), the displacement components are

$$u_\xi = \frac{Q}{2\pi G}\left(\frac{1}{\rho_1} - \nu\frac{\eta^2}{\rho_1^3} - \frac{1}{\rho_2} + \nu\frac{\eta^2}{\rho_2^3}\right),$$
$$u_\eta = \frac{Q\nu\eta}{2\pi G}\left(\frac{\xi - d/2}{\rho_1^3} - \frac{\xi + d/2}{\rho_2^3}\right), \tag{5}$$

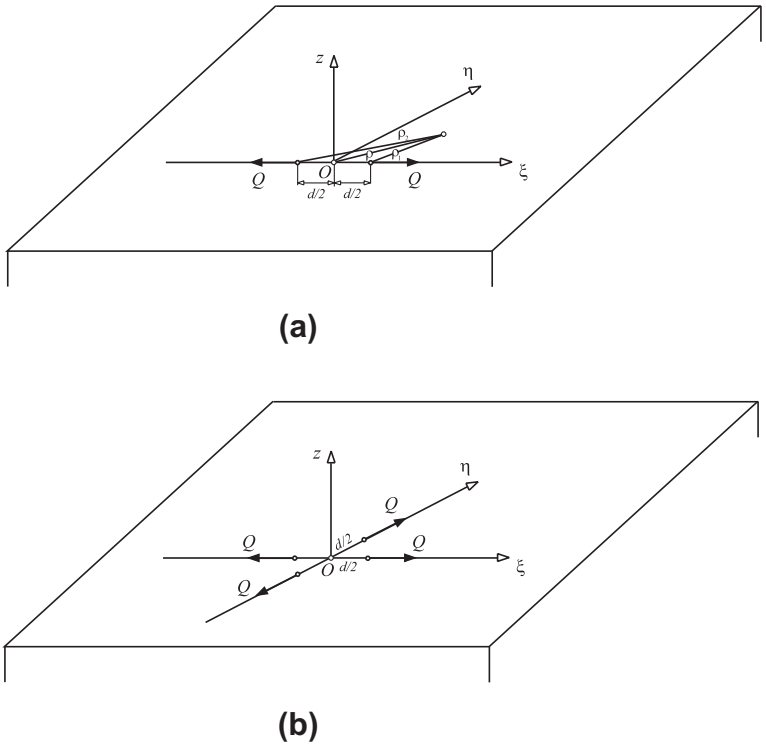

Fig. 2. (a) A doublet of two tangential forces Q on the surface of a half-space, at a small distance d along the ξ-axis. (b) A quadruplet of four tangential forces Q on the surface of a half-space. The distance between each pair of forces along the two coordinate axes is d.

$$u_z = -\frac{Q(1-2\nu)}{4\pi G}\left(\frac{\xi - d/2}{\rho_1^2} - \frac{\xi + d/2}{\rho_2^2}\right). \tag{6}$$

Sufficiently far from the center of the doublet, and to first order in d/ρ, the displacement components are

$$u_\xi = \frac{Qd}{2\pi G}\frac{\xi}{\rho^3}\left(1 - 3\nu\frac{\eta^2}{\rho^2}\right), \quad u_\eta = \frac{Qd}{2\pi G}\frac{\nu\eta}{\rho^3}\left(3\frac{\xi^2}{\rho^2} - 1\right), \tag{7}$$

$$u_z = -\frac{Qd(1-2\nu)}{4\pi G}\frac{1}{\rho^2}\left(2\frac{\xi^2}{\rho^2} - 1\right). \tag{8}$$

2.4. Surface quadruplet

The superposition of the doublets along the ξ and η-axis gives rise of a quadruplet, shown in Fig. 2(b). The surface displacement components are

$$u_\xi = \frac{Qd(1-\nu)}{2\pi G}\frac{\xi}{\rho^3}, \quad u_\eta = \frac{Qd(1-\nu)}{2\pi G}\frac{\eta}{\rho^3}, \quad u_z = 0. \tag{9}$$

The radial component of this displacement is

$$u_\rho = \frac{Qd(1-\nu)}{2\pi G}\frac{1}{\rho^2}. \tag{10}$$

The nonvanishing surface strains and stresses are

$$\epsilon_\rho = \frac{\mathrm{d}u_\rho}{\mathrm{d}\rho} = -\frac{Qd(1-\nu)}{\pi G}\frac{1}{\rho^3}, \quad \epsilon_\theta = \frac{u_\rho}{\rho} = \frac{Qd(1-\nu)}{2\pi G}\frac{1}{\rho^3}, \tag{11}$$

$$\sigma_\rho = -\sigma_\theta = -\frac{Qd(2-\nu)}{\pi}\frac{1}{\rho^3}. \tag{12}$$

3. Displacements due to vertical ring load

Fig. 3(a) shows the circular ring load on the surface of a half-space: the vertical line force V (per unit length) is applied along the circle of radius R. The magnitude of the total vertical force is $2\pi RV$. The vertical component of displacement of the points on the surface of a half-space ($z = 0$) can be obtained by integrating the contributions from the individual concentrated forces $VR\mathrm{d}\varphi$. By using the third expression in (1), this is

$$\mathrm{d}u_z = \frac{1-\nu}{2\pi G}\frac{VR\mathrm{d}\varphi}{\rho}, \tag{13}$$

where

$$\rho^2 = R^2 + r^2 - 2Rr\cos\varphi = (R+r)^2(1 - \hat{k}^2\sin^2\theta) \tag{14}$$

and

$$\theta = \frac{1}{2}(\pi - \varphi), \quad \hat{k}^2 = \frac{4Rr}{(R+r)^2} \leqslant 1. \tag{15}$$

The substitution of (14) into (13), and integration, gives

$$u_z = \frac{2V(1-\nu)}{\pi G}\frac{R}{R+r}K(\hat{k}), \quad K(\hat{k}) = \int_0^{\pi/2}\frac{\mathrm{d}\theta}{(1-\hat{k}^2\sin^2\theta)^{1/2}}, \tag{16}$$

where $K(\hat{k})$ denotes the complete elliptic integral of the first kind, in agreement with (3.96a) of Johnson (1985, p. 77).

The radial component of displacement of the points outside the ring load ($r > R$) is obtained from Fig. 3(b) by integrating the contributions $\mathrm{d}u_r = \mathrm{d}u_\xi$ at the point r due to all forces $VR\mathrm{d}\varphi$ applied along the circle of radius R. By using (1), this is

$$\mathrm{d}u_r = \frac{1-2\nu}{4\pi G}\frac{V(r - R\cos\varphi)R\mathrm{d}\varphi}{\rho^2}. \tag{17}$$

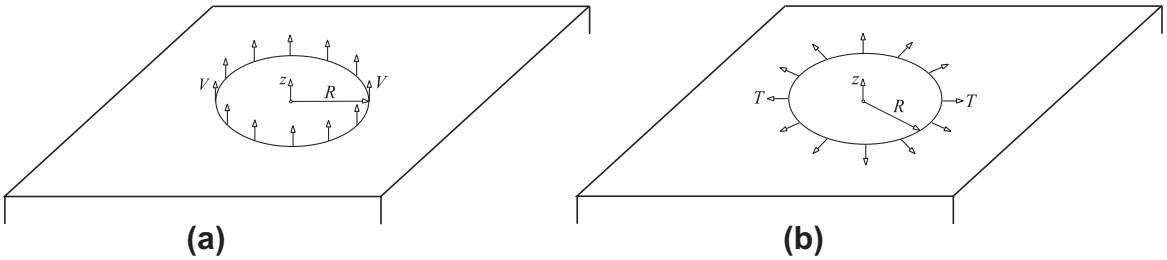

Fig. 3. (a) Vertical line load V, and (b) tangential (radial) line load T distributed on the surface of a half-space along the circle of radius R.

Upon integration, there follows

$$u_r = \frac{V(1-2\nu)}{2G}\frac{R}{r}. \tag{18}$$

Similar analysis applies for the points inside the ring load ($r < R$), with the end result $u_r = 0$. Thus, the radial displacement of the points on the surface of a half-space is

$$u_r = \frac{V(1-2\nu)}{2G}\begin{cases} 0, & r < R, \\ \frac{R}{r}, & r > R, \end{cases} \tag{19}$$

in agreement with (3.96b,c) of Johnson (1985, p. 77). The solution predicts the discontinuity in the radial displacement at $r = R$ of the magnitude $V(1-2\nu)/(2G)$.

If the line force V is compressive, rather than tensile, there would be an unphysical material interpenetration for

$$R < r < \frac{R}{2}\left[1 + \sqrt{1 + \frac{2V(1-2\nu)}{GR}}\right], \tag{20}$$

because the elasticity solution predicts in that region $|u(r)| > r - R$, while $u(r) = 0$ for $r < R$.

3.1. Alternative displacement expressions

3.1.1. Displacements of points outside the ring load

An alternative integration procedure yields another appealing representation of the displacement expressions. The contribution to vertical displacement from the two line load segments, one at the distance ρ and the other at the distance $\rho + b$ from the point r (Fig. 4(a)), at which the displacement is being calculated, is

$$\mathrm{d}u_z = \frac{V(1-\nu)}{2\pi G}\left(\frac{R\mathrm{d}\varphi_1}{\rho} + \frac{R\mathrm{d}\varphi_2}{\rho + b}\right). \tag{21}$$

Since, by the geometric considerations, $\rho \mathrm{d}\psi = R\mathrm{d}\varphi_1 \cos\varphi$ and $(\rho + b)\mathrm{d}\psi = R\mathrm{d}\varphi_2 \cos\varphi$, (21) can be rewritten as

$$\mathrm{d}u_z = \frac{V(1-\nu)}{\pi G}\frac{\mathrm{d}\psi}{\cos\varphi}. \tag{22}$$

The integration of (22) over the entire circle gives

$$u_z = \frac{2V(1-\nu)}{\pi G}\int_0^{\psi_1}\frac{\mathrm{d}\psi}{\cos\varphi}, \quad \sin\psi_1 = \frac{R}{r}. \tag{23}$$

By using the relationships $R\sin\varphi = r\sin\psi$ and $R\cos\varphi \mathrm{d}\varphi = r\cos\psi \mathrm{d}\psi$, (23) becomes

$$u_z = \frac{2V(1-\nu)}{\pi G}\frac{R}{r}\int_0^{\pi/2}\frac{\mathrm{d}\varphi}{\cos\psi}, \quad \cos\psi = \left(1 - \frac{R^2}{r^2}\sin^2\varphi\right)^{1/2}, \tag{24}$$

i.e.,

$$u_z = \frac{2V(1-\nu)}{\pi G}\frac{R}{r}K\left(\frac{R}{r}\right), \quad r \geqslant R. \tag{25}$$

For $r \gg R$, (25) reduces to

$$u_z = \frac{V(1-\nu)}{G}\frac{R}{r}, \quad r \gg R. \tag{26}$$

The same displacement would be produced by a concentrated force $Q_z = 2\pi RV$ applied at the origin $r = 0$; cf. (1).

The derivation of the expression for the radial displacement proceeds similarly, except that the Boussinesq component of the tangential displacement (in the ρ-direction) has to be projected into the r-direction, by multiplying it with $\cos\psi$. This gives

$$\mathrm{d}u_r = \frac{V(1-2\nu)}{4\pi G}\left(\frac{R\mathrm{d}\varphi_1}{\rho} + \frac{R\mathrm{d}\varphi_2}{\rho + b}\right)\cos\psi, \tag{27}$$

or, upon integration,

$$u_r = \frac{V(1-2\nu)}{2G}\frac{R}{r}, \quad r > R. \tag{28}$$

The same displacement (for $r > R$) would be produced by a concentrated force $Q_z = 2\pi RV$ applied at the origin $r = 0$; cf. (2).

3.1.2. Displacements of points inside the ring load

For the points inside the ring load ($r < R$), we have from Fig. 4(b),

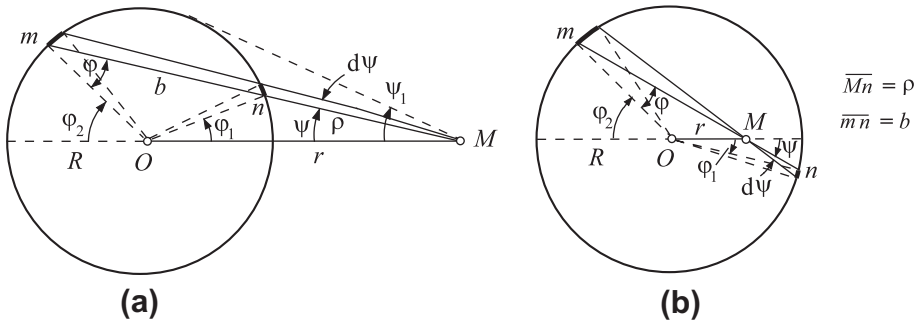

Fig. 4. (a) The geometrical construction used to derive the displacement at a point M outside the circular line load, by integrating the Boussinesq contributions from the two line force elements at m and n, at the distance ρ and $\rho + b$ from M. The length $\overline{mn} = b$. (b) The geometrical construction used to derive the displacement at a point M inside the circular line load. The two line force elements at m and n are at the distance ρ and $b - \rho$ from M.

$$\mathrm{d}u_z = \frac{V(1-\nu)}{2\pi G}\left(\frac{R\mathrm{d}\varphi_1}{\rho} + \frac{R\mathrm{d}\varphi_2}{b-\rho}\right). \tag{29}$$

Since $\rho \mathrm{d}\psi = R\mathrm{d}\varphi_1 \cos\varphi$ and $(b-\rho)\mathrm{d}\psi = R\mathrm{d}\varphi_2 \cos\varphi$, the substitution into (29) gives

$$\mathrm{d}u_z = \frac{V(1-\nu)}{\pi G}\frac{\mathrm{d}\psi}{\cos\varphi}, \quad \cos\varphi = \left(1 - \frac{r^2}{R^2}\sin^2\psi\right)^{1/2}. \tag{30}$$

By integrating, letting $\psi \in [0, \pi/2]$, and by multiplying the result with 2 to cover the entire circle, there follows

$$u_z = \frac{2V(1-\nu)}{\pi G} K\left(\frac{r}{R}\right), \quad r \leqslant R. \tag{31}$$

The displacement at the center is $u_z(0) = (1-\nu)V/G$.

Combined together, (25) and (31) yield

$$u_z = \frac{2V(1-\nu)}{\pi G}\begin{cases} \frac{R}{r}K\left(\frac{R}{r}\right), & r \geqslant R, \\ K\left(\frac{r}{R}\right), & r \leqslant R. \end{cases} \tag{32}$$

The corresponding plot is shown in Fig. 5(a). For better visualization of the deformed surface shape, the symmetric variation of the displacement along any two radial directions, opposite to each other, is shown (r/R thus being positive in both directions). The vertical displacement under the load is divergent, because $K(k) \to \infty$ as $k \to 1$.

To derive the radial displacement in the range $r < R$, we begin by superimposing the two Boussinesq contributions from the pair of forces,

$$\mathrm{d}u_r = \frac{V(1-2\nu)}{4\pi G}\left(\frac{R\mathrm{d}\varphi_2}{\rho+b} - \frac{R\mathrm{d}\varphi_1}{\rho}\right)\cos\psi. \tag{33}$$

This is identically equal to zero, and therefore the radial displacement vanishes at every point inside the ring load, i.e., $u_r = 0$ for $r < R$. By combining this with (28), we reproduce (19). The plot of $u = u_r(r)$ is shown in Fig. 5(b). There is a discontinuity in the radial displacement at $r = R$ of the amount $u_r(R^+) - u_r(R^-) = V(1-2\nu)/(2G)$. There is also a discontinuity in its gradient (radial strain), $(\mathrm{d}u_r/\mathrm{d}r)_{R^+} - (\mathrm{d}u_r/\mathrm{d}r)_{R^-} = -V(1-2\nu)/(2GR)$.

3.2. Transition from (16)–(25) and (31)

The transition from the vertical displacement expression (16) to its alternative representation as (25) and (31) follows by using the identity (Gradshteyn and Ruzhik, 1965, p. 908)

$$K\left(\frac{2\sqrt{k}}{1+k}\right) = (1+k)K(k). \tag{34}$$

If $r/R \leqslant 1$, the parameters k and $\hat{k}$ are related by

$$\hat{k}^2 = \frac{4Rr}{(R+r)^2} = \frac{4k}{(1+k)^2}, \quad k = \frac{r}{R} \leqslant 1 \tag{35}$$

and the substitution of (34) into (16) gives (31). On the other hand, if in the above expression $k = R/r \leqslant 1$, then the substitution of (34) into (16) reproduces (25).

3.3. Surface stress components

The nonvanishing strain components at the points of the surface of a half-space are calculated from (19) by using the expressions $\epsilon_r = \mathrm{d}u_r/\mathrm{d}r$ and $\epsilon_\theta = u_r/r$. This gives

$$\epsilon_r = -\epsilon_\theta = -\frac{V(1-2\nu)}{2GR}\begin{cases} 0, & r < R, \\ \frac{R^2}{r^2}, & r > R. \end{cases} \tag{36}$$

This being locally the state of simple shear, the corresponding surface stresses are

$$\sigma_r = -\sigma_\theta = -\frac{V(1-2\nu)}{R}\begin{cases} 0, & r < R, \\ \frac{R^2}{r^2}, & r > R. \end{cases} \tag{37}$$

The discontinuity of the stress components across the radius $r = R$ is of the magnitude $\sigma_0 = V(1-2\nu)/R$. The plots of the radial and circumferential stress components are shown in Fig. 6(a).

4. Displacements due to uniform tension within the circular area

Displacement components in the classical Love's (1929) problem of uniformly distributed normal load within a circular area on the surface of a half-space (Fig. 7(a)) can be easily derived by integrating the results for the circular ring load obtained in the previous section, and by using $p = V\mathrm{d}\rho$. The vertical displacement is

$$u_z = \frac{2p(1-\nu)}{\pi G}\left[\int_0^r K\left(\frac{r}{\rho}\right)\mathrm{d}\rho + \int_r^R \frac{\rho}{r}K\left(\frac{\rho}{r}\right)\mathrm{d}\rho\right], \quad r \leqslant R \tag{38}$$

and

$$u_z = \frac{2p(1-\nu)}{\pi G}\int_0^R K\left(\frac{r}{\rho}\right)\mathrm{d}\rho, \quad r \geqslant R. \tag{39}$$

Recalling that (Gradshteyn and Ruzhik, 1965, pp. 626–627)

$$\int kK(k)\mathrm{d}k = E(k) - (1-k^2)K(k), \quad \int K(k)\frac{\mathrm{d}k}{k^2} = -\frac{E(k)}{k}, \tag{40}$$

where $K(k)$ and $E(k)$ are the complete elliptic integrals of the first and second kind, from (38) and (39) there follows

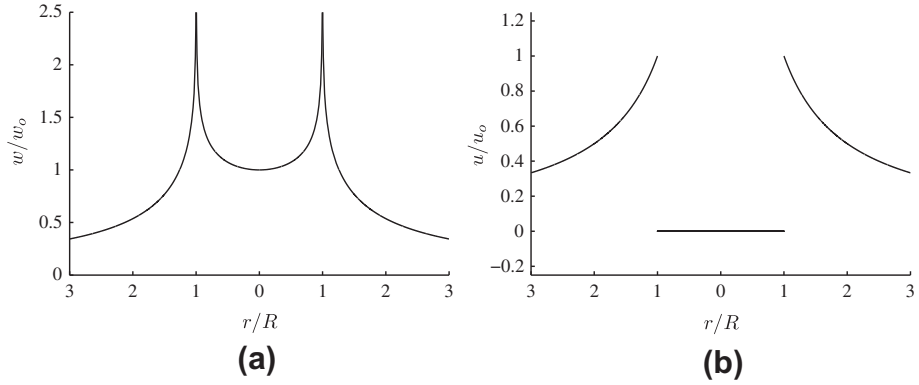

Fig. 5. (a) The vertical displacement of the surface of a half-space, $w = u_z(r)$, due to vertical circular line load V, normalized by $w_0 = V(1-\nu)/G$. (b) The corresponding radial displacement $u = u_r(r)$, normalized by $u_0 = V(1-2\nu)/(2G)$. The vertical displacement is singular, and the radial displacement is discontinuous at $r = R$.

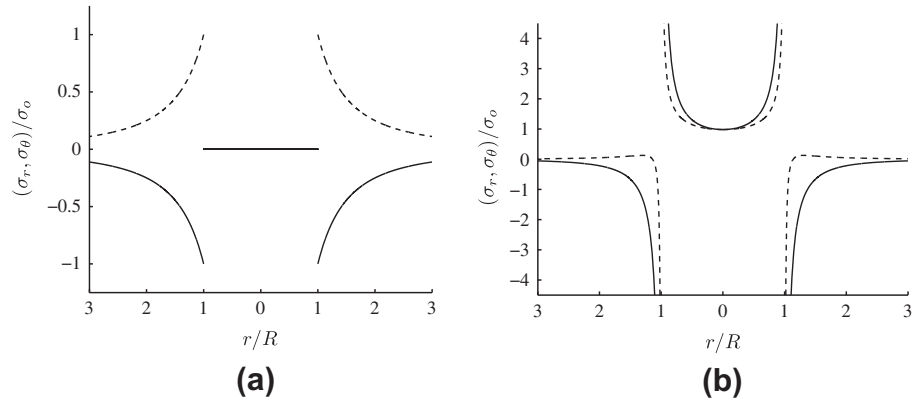

Fig. 6. The radial (solid line) and circumferential (dashed line) surface stresses $(\sigma_r, \sigma_\theta)$ due to: (a) vertical ring load V from Fig. 3(a), normalized by $\sigma_0 = V(1-2\nu)/R$, and (b) tangential ring load from Fig. 3(b), normalized by $\sigma_0 = 4T/(\pi R)$. The Poisson ratio is taken to be $\nu = 0.25$.

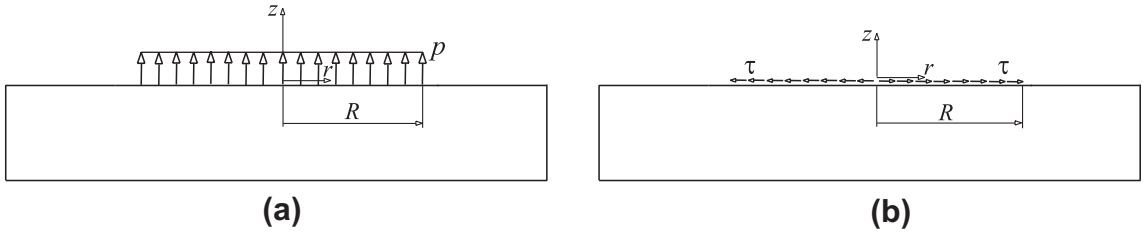

Fig. 7. The uniform (a) tension p and (b) radial shear stress τ applied on the surface of a half-space within a circular area of radius R.

$$u_z = \frac{2pR(1-\nu)}{\pi G}\begin{cases} E\left(\frac{r}{R}\right), & r \leqslant R, \\ \frac{r}{R}\left[E\left(\frac{R}{r}\right) - \left(1-\frac{R^2}{r^2}\right)K\left(\frac{R}{r}\right)\right], & r \geqslant R, \end{cases} \tag{41}$$

in agreement with Timoshenko and Goodier (1970, p. 404), or Johnson (1985, pp. 57–58). The elevation at the center is $u_z(0) = (1-\nu)pR/G$. Fig. 8(a) shows the variation of the vertical displacement $w = u_z(r)$. There is a singularity in the slope $\mathrm{d}u_z/\mathrm{d}r$ at $r = R$. Since $\epsilon_{zr} = 0$ on the surface of the substrate, the singularity of $\partial u_z/\partial r$ at $r = R$ is canceled by an opposite singularity of the gradient $\partial u_r/\partial z$ at $r = R$.

Similarly, by integrating (19), the radial displacement is found to be

$$u_r = \frac{p(1-2\nu)R}{4G}\begin{cases} \frac{r}{R}, & r \leqslant R, \\ \frac{R}{r}, & r \geqslant R, \end{cases} \tag{42}$$

as in Johnson (1985, p. 58).

There is a singular feature of the radial displacement, which itself is continuous at $r = R$, but its slope is not, because of the load discontinuity at $r = R$. This slope (radial strain) discontinuity is

$$\left(\frac{\mathrm{d}u_r}{\mathrm{d}r}\right)_{r=R^+} - \left(\frac{\mathrm{d}u_r}{\mathrm{d}r}\right)_{r=R^-} = -\frac{p(1-2\nu)}{2G}. \tag{43}$$

The plot of $u = u_r(r)$ is shown in Fig. 8(b). There is a discontinuity in the radial strain $\mathrm{d}u_r/\mathrm{d}r$ at $r = R$, because the applied tension abruptly changes from p to 0 across $r = R$.

4.1. Surface stress components

The radial displacement, together with Hooke's law, completely determines the nonvanishing strain components on the surface of a half-space. These are

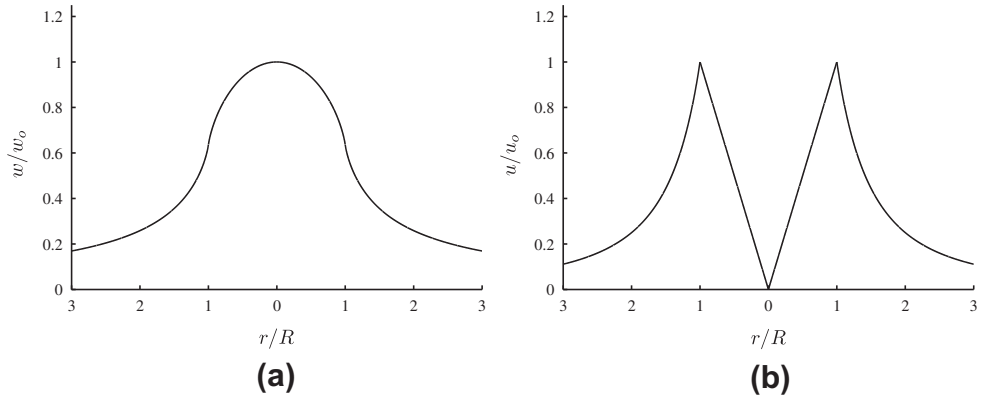

Fig. 8. (a) The vertical displacement $w = u_z(r)$ due to uniform tension p over the circular region of radius R, normalized by $w_0 = pR(1-\nu)/G$, as determined from (41). (b) The corresponding radial displacement $u = u_r(r)$, normalized by $u_0 = pR(1-\nu)/(4G)$, as determined from (42).

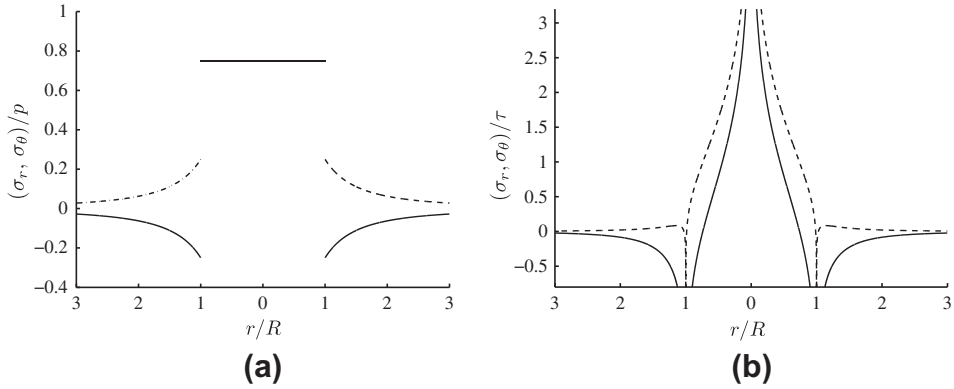

Fig. 9. The radial (solid line) and circumferential (dashed line) surface stresses $(\sigma_r, \sigma_\theta)$ for: (a) tension loading from Fig. 7(a), and (b) radial shear loading from Fig. 7(b). The Poisson ratio is $\nu = 0.25$.

$$\epsilon_r = \frac{\mathrm{d}u_r}{\mathrm{d}r}, \quad \epsilon_\theta = \frac{u_r}{r}, \quad \epsilon_z = \frac{1-2\nu}{2G(1-\nu)}\sigma_z - \frac{\nu}{1-\nu}(\epsilon_r + \epsilon_\theta). \tag{44}$$

Thus, in view of (42), the radial and circumferential surface strains are

$$\epsilon_r = \frac{p(1-2\nu)}{4G}\begin{cases} 1, & r < R, \\ -\frac{R^2}{r^2}, & r > R, \end{cases}; \quad \epsilon_\theta = \frac{p(1-2\nu)}{4G}\begin{cases} 1, & r < R, \\ \frac{R^2}{r^2}, & r > R. \end{cases} \tag{45}$$

The longitudinal stress and strain are

$$\sigma_z = p\begin{cases} 1, & r < R, \\ 0, & r > R, \end{cases}; \quad \epsilon_z = \frac{p(1-2\nu)}{2G}\begin{cases} 1, & r < R, \\ 0, & r > R. \end{cases} \tag{46}$$

The radial and circumferential stress components on the surface of a half-space are obtained from Hooke's law as

$$\sigma_r = \frac{2G}{1-\nu}(\epsilon_r + \nu\epsilon_\theta) + \frac{\nu}{1-\nu}\sigma_z, \quad \sigma_\theta = \frac{2G}{1-\nu}(\epsilon_\theta + \nu\epsilon_r) + \frac{\nu}{1-\nu}\sigma_z.$$

Upon the substitution of (45) and (46), this gives

$$\sigma_r = \frac{p}{2}\begin{cases} 1+2\nu, & r < R, \\ -(1-2\nu)\frac{R^2}{r^2}, & r > R, \end{cases}; \quad \sigma_\theta = \frac{p}{2}\begin{cases} 1+2\nu, & r < R, \\ (1-2\nu)\frac{R^2}{r^2}, & r > R. \end{cases} \tag{47}$$

The discontinuities in the surface stress components across the radius $r = R$ are

$$\sigma_r(R^+) - \sigma_r(R^-) = -p, \quad \sigma_\theta(R^+) - \sigma_\theta(R^-) = -2\nu p,$$
$$\sigma_z(R^+) - \sigma_z(R^-) = -p. \tag{48}$$

The plots of the radial and circumferential stress components are shown in Fig. 9(a). Both, the radial and circumferential stresses for $r < R$ are constant and equal to $(1+2\nu)p/2$. The presence of the stress discontinuity across $r = R$ was originally pointed out by Love (1929, p. 382). In the two-dimensional/plane version of the considered problem, the longitudinal surface stress just below the ends of the loading interval is also discontinuous, the magnitude of the discontinuity being equal to p.

4.2. From uniform tension to ring load

The expression for u_z^V can be obtained from the expression for u_z^p by superimposing the solutions of two loadings on the surface of a half-space, and by performing an appropriate limit. These loadings are the pressure of magnitude p over the circle of radius R, and the tension of magnitude p over the circle of radius $R + \Delta R$ ($\Delta R \ll R$). The resulting displacement is[1]

$$u_z^V(r) = \frac{\mathrm{d}u_z^p}{\mathrm{d}R}\Delta R, \quad p\Delta R \to V, \tag{49}$$

to first order in ΔR. By using (41) for u_z^p, and by recalling that (Gradshteyn and Ruzhik, 1965, p. 907)

$$\frac{\mathrm{d}E(k)}{\mathrm{d}k} = \frac{1}{k}[E(k) - K(k)], \quad \frac{\mathrm{d}K(k)}{\mathrm{d}k} = \frac{1}{k}\left[\frac{E(k)}{1-k^2} - K(k)\right], \tag{50}$$

it follows that

$$u_z^V = \frac{2(1-\nu)V}{\pi G}\begin{cases} K(\frac{r}{R}), & r \leqslant R, \\ \frac{R}{r}K(\frac{R}{r}), & r \geqslant R, \end{cases} \tag{51}$$

reproducing (25) and (31).

Similarly, the radial displacement (19) due to tensile line load V can be deduced from (42) in the limit

$$u_r^V = \lim_{p\Delta R \to V}\left(\frac{\mathrm{d}u_r^p}{\mathrm{d}R}\Delta R\right) = \frac{V(1-2\nu)}{2G}\begin{cases} 0 & r < R, \\ \frac{R}{r}, & r > R. \end{cases} \tag{52}$$

5. Tension load over an annular ring

To eliminate the singularity of displacement under the circular line load, it is assumed that the vertical load is distributed over a small but finite thickness. The vertical displacement along the surface of the substrate due to the loading shown in Fig. 10(a) is readily obtained from (28) by superposing the displacements due to tensile load of magnitude p along $r \leqslant R$ and the pressure load of magnitude p along $r \leqslant R_0$. This gives

$$u_z = \frac{2(1-\nu)pR}{\pi G}U_z, \tag{53}$$

[1] This simple method of calculating the surface displacement due to circular line load can be used for other problems, as well (circular plates, cylindrical shells, beams on elastic foundation, etc.). For example, in the Euler–Bernoulli beam theory, the deflection of the cantilever beam of length L due to the concentrated force F at its end can be calculated from $(\mathrm{d}w^p/\mathrm{d}L)\Delta L$, in the limit as $p\Delta L \to F$, where $w^p = px^2(6L^2 - 4Lx + x^2)/(24EI)$ is the deflection due to uniform pressure p over the entire length of the cantilever. The bending stiffness of the beam is EI, and x is the running coordinate along its length measured from the fixed end.

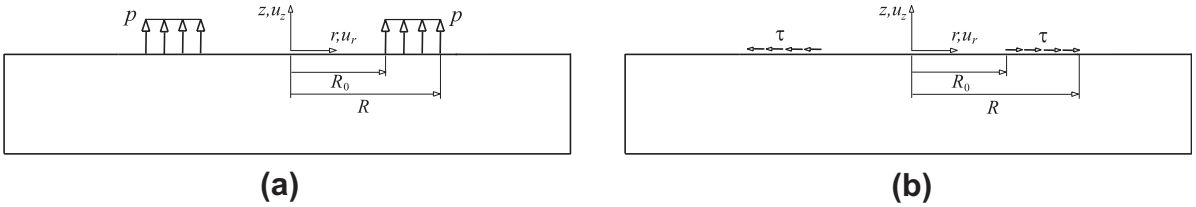

Fig. 10. The uniform (a) tension p and (b) radial shear stress τ applied within the annular region $R_0 \leqslant r \leqslant R$ on the surface of a half-space.

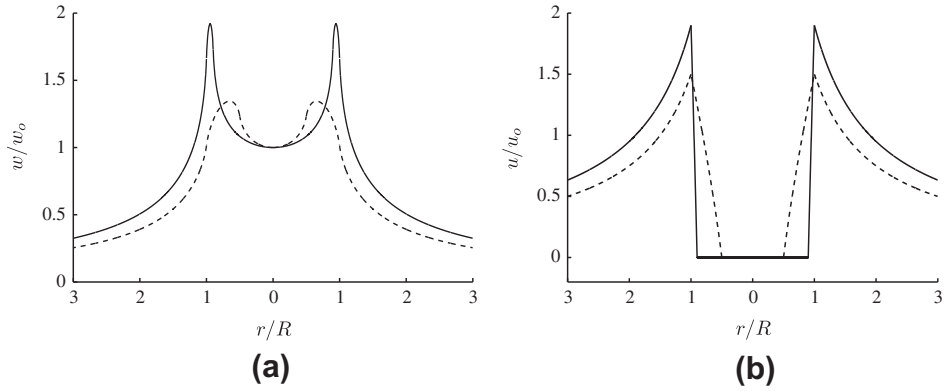

Fig. 11. (a) The vertical displacement $w = u_z(r)$ along the surface of the substrate for the loading shown in Fig. 10(a). The solid curve is for $R_0 = 0.9R$, and the dotted for $R_0 = 0.5R$. The normalizing displacement factor is $w_0 = (1-\nu)p(R-R_0)/G$. (b) The corresponding radial displacement $u = u_r(r)$. The normalizing displacement factor is $u_0 = (1-2\nu)p(R-R_0)/(4G)$.

with

$$U_z = \begin{cases} E\left(\frac{r}{R}\right) - \frac{R_0}{R}E\left(\frac{r}{R_0}\right), & r \leqslant R_0, \\ E\left(\frac{r}{R}\right) - \frac{r}{R}\left[E\left(\frac{R_0}{r}\right) - \left(1 - \frac{R_0^2}{r^2}\right)K\left(\frac{R_0}{r}\right)\right], & R_0 \leqslant r \leqslant R, \\ \frac{r}{R}\left[E\left(\frac{R}{r}\right) - E\left(\frac{R_0}{r}\right) - \left(1 - \frac{R^2}{r^2}\right)K\left(\frac{R}{r}\right) + \left(1 - \frac{R_0^2}{r^2}\right)K\left(\frac{R_0}{r}\right)\right], & r \geqslant R. \end{cases}$$

The corresponding radial displacement is obtained in the same way by using (42), with the end result

$$u_r = \frac{p(1-2\nu)r}{4G}\begin{cases} 0, & r \leqslant R_0, \\ 1 - \frac{R_0^2}{r^2}, & R_0 \leqslant r \leqslant R, \\ \frac{R^2 - R_0^2}{r^2}, & r \geqslant R. \end{cases} \tag{54}$$

Fig. 11(a) shows the vertical displacement profile $w = u_z(r)$ in the cases $R - R_0 = 0.1R$ and $0.5R$. The plots show the formation of a blunted ridge under the load. As expected, the blunting increases with the increase of the interface thickness $R - R_0$. Fig. 11(b) shows the corresponding radial displacement $u = u_r(r)$. In the limit as $r \to \infty$, the radial displacement vanishes. The displacement gradient is discontinuous at $r = R_0$ and $r = R$. There is a sharp displacement gradient $\mathrm{d}u_r/\mathrm{d}r$ between $r = R_0$ and $r = R$, which is sharper for the smaller width $(R - R_0)$, giving rise to displacement discontinuity of amount $V(1-2\nu)/(2G)$ in the limit as $R \to R_0$ and $p(R - R_0) \to V$; cf. Fig. 5(b).

5.1. Surface stress components

The radial and circumferential strain components are, from (44) and (54),

$$(\epsilon_r, \epsilon_\theta) = \frac{p(1-2\nu)}{4G}\begin{cases} 0, & r < R_0, \\ 1 \pm \frac{R_0^2}{r^2}, & R_0 < r < R, \\ \mp\frac{R^2 - R_0^2}{r^2}, & r > R. \end{cases} \tag{55}$$

The longitudinal stress and strain are

$$\sigma_z = p\begin{cases} 0, & r < R_0, \\ 1, & R_0 < r < R, \\ 0, & r > R, \end{cases}; \quad \epsilon_z = \frac{p(1-2\nu)}{2G}\begin{cases} 0, & r < R_0, \\ 1, & R_0 < r < R, \\ 0, & r > R. \end{cases} \tag{56}$$

The corresponding radial and circumferential stresses on the surface of a half-space follow from Hooke's law as

$$(\sigma_r, \sigma_\theta) = \frac{p}{2}\begin{cases} 0, & r < R_0, \\ 1 + 2\nu \pm (1-2\nu)\frac{R_0^2}{r^2}, & R_0 < r < R, \\ \mp(1-2\nu)\frac{R^2 - R_0^2}{r^2}, & r > R. \end{cases} \tag{57}$$

The discontinuities in the surface stress components across the radii $r = R_0$ and $r = R$ are

$$\begin{aligned} &\sigma_r(R_0^+) - \sigma_r(R_0^-) = p, \quad \sigma_r(R^+) - \sigma_r(R^-) = -p, \\ &\sigma_\theta(R_0^+) - \sigma_\theta(R_0^-) = 2\nu p, \quad \sigma_\theta(R^+) - \sigma_\theta(R^-) = -2\nu p. \end{aligned} \tag{58}$$

The radial and circumferential stresses are plotted in Fig. 12(a). The stress discontinuities would be eliminated if the applied load p has gradually rather than abruptly decreased to zero at the boundaries of the loading annulus.

6. Tangential line load

Fig. 3(b) shows a tangential line load (T) in the radial direction along the circle of radius R. Two different representations of the expressions for the displacement components on the surface of a half-space are derived in this section.

Radial displacement

The contribution to radial displacement at the point r from the tangential force $TR\mathrm{d}\varphi$ at an arbitrary point (R, φ) (Fig. 13) is $\mathrm{d}u_r = \mathrm{d}u_\xi \cos\varphi - \mathrm{d}u_\eta \sin\varphi$, where, by using (4),

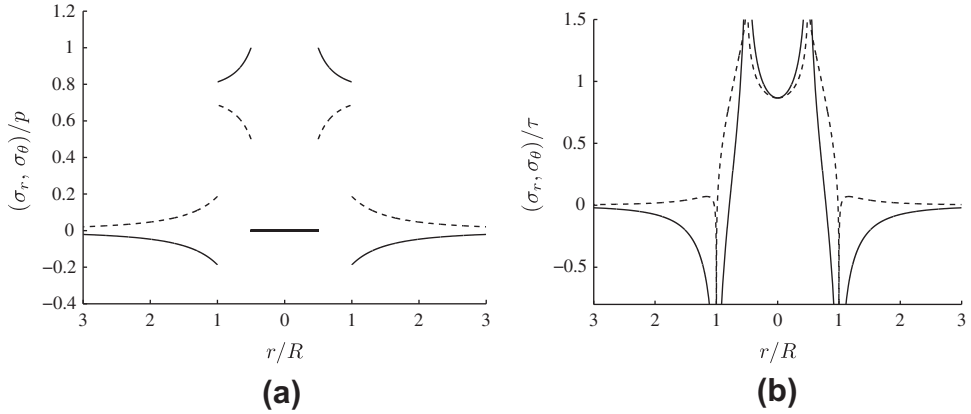

Fig. 12. The radial (solid line) and circumferential (dashed line) surface stresses $(\sigma_r, \sigma_\theta)$ for: (a) annular vertical load from Fig. 10(a), and (b) radial shear load from Fig. 10(b). The radius $R_0 = 0.5R$ and the Poisson ratio is $\nu = 0.25$.

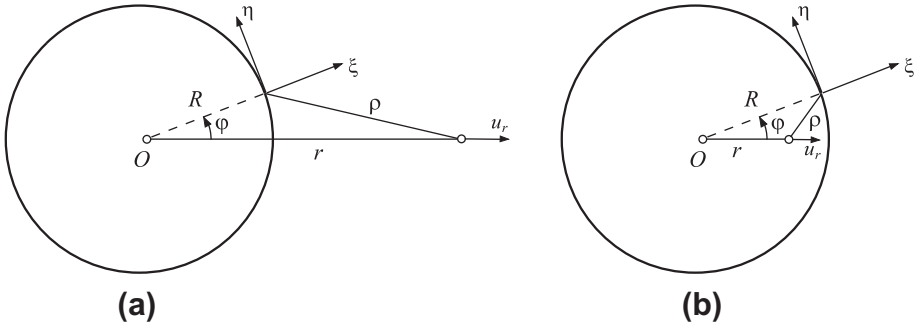

Fig. 13. The calculation of the radial displacement u_r at an arbitrary point at distance r from the origin O, in case (a) $r > R$, and (b) $r < R$. The result is obtained by integrating the contributions from the radial force $TR\mathrm{d}\varphi$ at an arbitrary point (R, φ) along the circle of radius R. The local coordinate axes at that point are (ξ, η).

$$\mathrm{d}u_\xi = \frac{TR\mathrm{d}\varphi}{2\pi G}\left[\frac{1}{\rho} - \nu\frac{(r\sin\varphi)^2}{\rho^3}\right], \quad \mathrm{d}u_\eta = \frac{TR\mathrm{d}\varphi}{2\pi G}\frac{\nu r\sin\varphi(R - r\cos\varphi)}{\rho^3}. \tag{59}$$

Thus,

$$\mathrm{d}u_r = \frac{TR\mathrm{d}\varphi}{2\pi G}\left(\frac{1}{\rho}\cos\varphi - \nu Rr\frac{\sin^2\varphi}{\rho^3}\right). \tag{60}$$

Since

$$\rho^2 = R^2 + r^2 - 2Rr\cos\varphi = (R+r)^2(1 - \hat{k}^2\sin^2\theta) \tag{61}$$

and

$$\theta = \frac{1}{2}(\pi - \varphi), \quad \hat{k}^2 = \frac{4Rr}{(R+r)^2} \leqslant 1, \tag{62}$$

the expression (60) can be rewritten as

$$\mathrm{d}u_r = \frac{-TR\mathrm{d}\theta}{\pi G(R+r)}\left[\frac{2\sin^2\theta - 1}{(1 - \hat{k}^2\sin^2\theta)^{1/2}} - \frac{4\nu Rr}{(R+r)^2}\frac{\sin^2\theta\cos^2\theta}{(1 - \hat{k}^2\sin^2\theta)^{3/2}}\right]. \tag{63}$$

Recalling that (Gradshteyn and Ruzhik, 1965, pp. 162 and 165)

$$\begin{aligned} &\int_0^{\pi/2}\frac{\sin^2\theta\mathrm{d}\theta}{(1-\hat{k}^2\sin^2\theta)^{1/2}} = \frac{1}{\hat{k}^2}[K(\hat{k}) - E(\hat{k})], \\ &\int_0^{\pi/2}\frac{\sin^2\theta\cos^2\theta\mathrm{d}\theta}{(1-\hat{k}^2\sin^2\theta)^{3/2}} = \frac{1}{\hat{k}^4}[(2-\hat{k}^2)K(\hat{k}) - 2E(\hat{k})], \end{aligned} \tag{64}$$

the integration of (63) gives

$$u_r = \frac{T(1-\nu)}{\pi G}\frac{R+r}{r}\left[\left(1 - \frac{1}{2}\hat{k}^2\right)K(\hat{k}) - E(\hat{k})\right], \tag{65}$$

in agreement with (3.97a) of Johnson (1985, p. 77).

Vertical displacement

The vertical component of displacement of the points outside the ring load ($r > R$) is obtained from Fig. 13(a) by integrating the contributions from the third of (4) corresponding to the radial force $TR\mathrm{d}\varphi$. This is

$$\mathrm{d}u_z = -\frac{1-2\nu}{4\pi G}\frac{T(r\cos\varphi - R)R\mathrm{d}\varphi}{\rho^2}. \tag{66}$$

Introducing the angle $\theta = (\pi - \varphi)/2$, the above can be recast as

$$\mathrm{d}u_z = \frac{TR(1-2\nu)}{2\pi G}\frac{2r\sin^2\theta - (r+R)}{(R+r)^2(1 - \hat{k}^2\sin^2\theta)}\mathrm{d}\theta. \tag{67}$$

Upon the integration, following the same procedure as in Section 3, it follows that $u_z = 0$.

For the points inside the ring load (Fig. 13(b)), the same analysis applies, except that in the integration procedure $(1 - \hat{k}^2)^{1/2} = (R - r)/(R + r)$. The end result is $u_z = T(1 - 2\nu)/(2G)$. Thus, the vertical displacement of the points on the surface of a half-space due to tangential ring load T is

$$u_z = \frac{T(1-2\nu)}{2G}\begin{cases} 1, & r < R, \\ 0, & r > R, \end{cases} \tag{68}$$

in agreement with (3.97b,c) of Johnson (1985, p. 77).

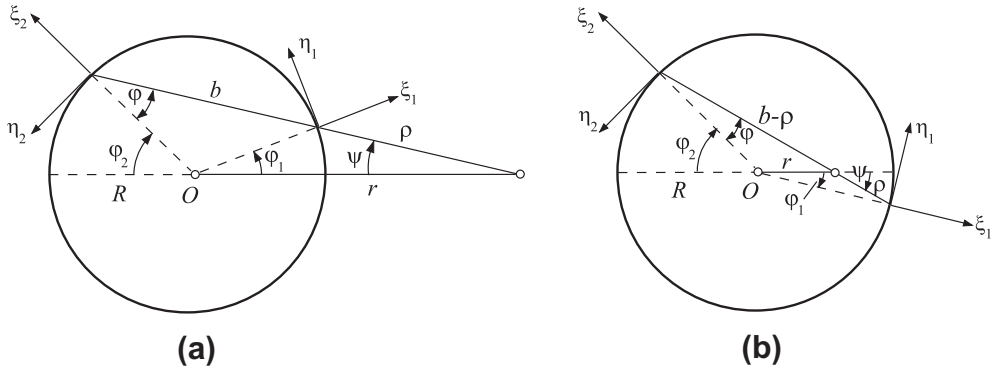

Fig. 14. The geometric construction used to derive the displacement components by integrating the Cerruti contributions from the two line segments at the distance ρ and (a) $b+\rho$, or (b) $b-\rho$ from the point at which the displacement is being calculated.

6.1. Alternative displacement expressions

6.1.1. Displacements of points outside the ring load

An alternative derivation proceeds by considering the contribution to radial displacement from two line load segments, one at the distance ρ and the other at the distance $\rho+b$ from the point r (Fig. 14(a)), at which the radial displacement is being calculated. This is

$$\mathrm{d}u_r = \mathrm{d}u_{\xi_1}\cos\varphi_1 - \mathrm{d}u_{\eta_1}\sin\varphi_1 - \mathrm{d}u_{\xi_2}\cos\varphi_2 - \mathrm{d}u_{\eta_2}\sin\varphi_2, \tag{69}$$

where

$$\mathrm{d}u_{\xi_1} = \frac{TR\mathrm{d}\varphi_1}{2\pi G}\left[\frac{1}{\rho} - \nu\frac{(\rho\sin\varphi)^2}{\rho^3}\right],$$

$$\mathrm{d}u_{\eta_1} = -\frac{TR\mathrm{d}\varphi_1}{2\pi G}\frac{\nu\rho^2\sin\varphi\cos\varphi}{\rho^3},$$

$$\mathrm{d}u_{\xi_2} = \frac{TR\mathrm{d}\varphi_2}{2\pi G}\left[\frac{1}{\rho+b} - \nu\frac{(\rho+b)^2\sin^2\varphi}{(\rho+b)^3}\right],$$

$$\mathrm{d}u_{\eta_2} = \frac{TR\mathrm{d}\varphi_2}{2\pi G}\frac{\nu(\rho+b)^2\sin\varphi\cos\varphi}{(\rho+b)^3}.$$

Since, by the geometric considerations,

$$\rho\mathrm{d}\psi = R\mathrm{d}\varphi_1\cos\varphi, \quad (\rho+b)\mathrm{d}\psi = R\mathrm{d}\varphi_2\cos\varphi,$$

$$r\sin\psi = R\sin\varphi, \quad \cos\psi = \left(1-\frac{R^2}{r^2}\sin^2\varphi\right)^{1/2},$$

$$\sin\varphi_1 = \frac{\rho}{R}\sin\psi, \quad \sin\varphi_2 = \frac{\rho+b}{R}\sin\psi,$$

$$\rho = r\cos\psi - R\cos\varphi, \quad \rho+b = r\cos\psi + R\cos\varphi$$

and since $\varphi_1 = \varphi-\psi$, $\varphi_2 = \varphi+\psi$, there follows

$$\mathrm{d}u_r = \frac{T(1-\nu)}{\pi G}\frac{R^2}{r^2}\frac{\sin^2\varphi}{\cos\psi}\mathrm{d}\varphi. \tag{70}$$

Upon the integration of (70), the radial displacement is found to be

$$u_r = \frac{2T(1-\nu)}{\pi G}\left[K\left(\frac{R}{r}\right) - E\left(\frac{R}{r}\right)\right], \quad r \geqslant R. \tag{71}$$

At large $r \gg R$, (71) gives

$$u_r(r) = \frac{T(1-\nu)}{2G}\frac{R^2}{r^2}, \quad r \gg R. \tag{72}$$

This also follows directly from the expression (10) for the radial displacement due to the force quadruplet, provided that the substitutions are made $Q = TR(\pi/2)$ and $d = 2R$.

6.1.2. Displacements of points inside the ring load

For the points insider the ring load ($r < R$), from Fig. 14(b) we have

$$\mathrm{d}u_r = \mathrm{d}u_{\xi_1}\cos\varphi_1 + \mathrm{d}u_{\eta_1}\sin\varphi_1 - \mathrm{d}u_{\xi_2}\cos\varphi_2 - \mathrm{d}u_{\eta_2}\sin\varphi_2, \tag{73}$$

where

$$\mathrm{d}u_{\xi_1} = \frac{TR\mathrm{d}\varphi_1}{2\pi G}\left[\frac{1}{\rho} - \nu\frac{(\rho\sin\varphi)^2}{\rho^3}\right],$$

$$\mathrm{d}u_{\eta_1} = -\frac{TR\mathrm{d}\varphi_1}{2\pi G}\frac{\nu\rho^2\sin\varphi\cos\varphi}{\rho^3},$$

$$\mathrm{d}u_{\xi_2} = \frac{TR\mathrm{d}\varphi_2}{2\pi G}\left[\frac{1}{b-\rho} - \nu\frac{(b-\rho)^2\sin^2\varphi}{(b-\rho)^3}\right],$$

$$\mathrm{d}u_{\eta_2} = \frac{TR\mathrm{d}\varphi_2}{2\pi G}\frac{\nu(b-\rho)^2\sin\varphi\cos\varphi}{(b-\rho)^3}.$$

Since

$$\rho\mathrm{d}\psi = R\mathrm{d}\varphi_1\cos\varphi, \quad (b-\rho)\mathrm{d}\psi = R\mathrm{d}\varphi_2\cos\varphi,$$

$$r\sin\psi = R\sin\varphi, \quad \cos\varphi = \left(1-\frac{r^2}{R^2}\sin^2\psi\right)^{1/2},$$

$$\sin\varphi_1 = \frac{\rho}{R}\sin\psi, \quad \sin\varphi_2 = \frac{b-\rho}{R}\sin\psi,$$

$$\rho = R\cos\varphi - r\cos\psi, \quad b-\rho = R\cos\varphi + r\cos\psi$$

and since $\varphi_1 = \psi-\varphi$, $\varphi_2 = \psi+\varphi$, there follows

$$\mathrm{d}u_r = \frac{T(1-\nu)}{\pi G}\frac{r}{R}\frac{\sin^2\psi}{\cos\varphi}\mathrm{d}\psi. \tag{74}$$

Thus, upon the integration,

$$u_r = \frac{2T(1-\nu)}{\pi G}\frac{R}{r}\left[K\left(\frac{r}{R}\right) - E\left(\frac{r}{R}\right)\right], \quad r \leqslant R. \tag{75}$$

Written together, expressions (71) and (75) are

$$u_r = \frac{2T(1-\nu)}{\pi G}\begin{cases}\frac{R}{r}\left[K\left(\frac{r}{R}\right) - E\left(\frac{r}{R}\right)\right], & r \leqslant R,\\ K\left(\frac{R}{r}\right) - E\left(\frac{R}{r}\right), & r \geqslant R.\end{cases} \tag{76}$$

The transition from the expression for the radial displacement (65) to its alterative representation (76) is made by using the relations (Gradshteyn and Ruzhik, 1965, p. 908)

$$K\left(\frac{2\sqrt{k}}{1+k}\right)=(1+k)K(k),\quad E\left(\frac{2\sqrt{k}}{1+k}\right)=\frac{1}{1+k}\left[2E(k)-(1-k^2)K(k)\right]. \tag{77}$$

6.1.3. Vertical displacement

For the points inside the ring load ($r<R$), we have

$$\mathrm{d}u_z=-\frac{TR\mathrm{d}\varphi_1}{4\pi G}(1-2\nu)\frac{-\rho\cos\varphi}{\rho^2}-\frac{TR\mathrm{d}\varphi_2}{4\pi G}(1-2\nu)\times\frac{-(b-\rho)\cos\varphi}{(b-\rho)^2}. \tag{78}$$

Since $\rho\mathrm{d}\psi=R\mathrm{d}\varphi_1\cos\varphi$ and $(b-\rho)\mathrm{d}\psi=R\mathrm{d}\varphi_2\cos\varphi$, the expression (78) becomes $\mathrm{d}u_z=T(1-2\nu)\mathrm{d}\psi/(2\pi G)$, and the integration gives

$$u_z=\frac{T(1-2\nu)}{2G},\quad r<R. \tag{79}$$

For the points outside the ring load ($r>R$),

$$\mathrm{d}u_z=-\frac{TR\mathrm{d}\varphi_1}{4\pi G}(1-2\nu)\frac{\rho\cos\varphi}{\rho^2}-\frac{TR\mathrm{d}\varphi_2}{4\pi G}(1-2\nu)\times\frac{-(b+\rho)\cos\varphi}{(b+\rho)^2}. \tag{80}$$

Since $\rho\mathrm{d}\psi=R\mathrm{d}\varphi_1\cos\varphi$ and $(b+\rho)\mathrm{d}\psi=R\mathrm{d}\varphi_2\cos\varphi$, the expression (80) reduces to $\mathrm{d}u_z=0$, i.e., upon integration, $u_z=0$ for $r>R$. Together, this and (79) reproduce (68). Fig. 15(b) shows the plot of the vertical displacement $w=u_z(r)$, normalized by $w_0=T(1-2\nu)/(2G)$. The parameter w_0 represents the vertical displacement for $r<R$, and thus the vertical displacement discontinuity across the radius $r=R$.

In retrospect, the result $u_z=0$ for $r>R$ could have been recognized from the outset by recalling that the vertical displacement of the points on the surface of a half-space due to the force quadruplet from Fig. 2(b) vanishes; cf. (9).

6.2. Surface stress components

The nonvanishing strain components at the points of the surface of a half-space are calculated from (76) by using the expressions $\epsilon_r=\mathrm{d}u_r/\mathrm{d}r$ and $\epsilon_\theta=u_r/r$. This gives

$$\epsilon_r=\frac{2T(1-\nu)}{\pi Gr}\begin{cases}\frac{Rr}{R^2-r^2}E\left(\frac{r}{R}\right)-\frac{R}{r}\left[K\left(\frac{r}{R}\right)-E\left(\frac{r}{R}\right)\right], & r<R,\\ -\frac{R^2}{r^2-R^2}E\left(\frac{R}{r}\right), & r>R\end{cases} \tag{81}$$

and

$$\epsilon_\theta=\frac{2T(1-\nu)}{\pi Gr}\begin{cases}\frac{R}{r}\left[K\left(\frac{r}{R}\right)-E\left(\frac{r}{R}\right)\right], & r<R,\\ K\left(\frac{R}{r}\right)-E\left(\frac{R}{r}\right), & r>R.\end{cases} \tag{82}$$

The corresponding surface stresses follow from Hooke's law as

$$\sigma_r=\frac{4T}{\pi r}\begin{cases}\frac{Rr}{R^2-r^2}E\left(\frac{r}{R}\right)-(1-\nu)\frac{R}{r}\left[K\left(\frac{r}{R}\right)-E\left(\frac{r}{R}\right)\right], & r<R,\\ -\frac{R^2}{r^2-R^2}E\left(\frac{R}{r}\right)+\nu\left[K\left(\frac{R}{r}\right)-E\left(\frac{R}{r}\right)\right], & r>R\end{cases} \tag{83}$$

and

$$\sigma_\theta=\frac{4T}{\pi r}\begin{cases}\frac{\nu Rr}{R^2-r^2}E\left(\frac{r}{R}\right)+(1-\nu)\frac{R}{r}\left[K\left(\frac{r}{R}\right)-E\left(\frac{r}{R}\right)\right], & r<R,\\ -\frac{\nu R^2}{r^2-R^2}E\left(\frac{R}{r}\right)+K\left(\frac{R}{r}\right)-E\left(\frac{R}{r}\right). & r>R.\end{cases} \tag{84}$$

The plots of the radial and circumferential stress components are shown in Fig. 6(b). The stresses are discontinuous and singular at $r=R$. The radial stress is tensile for $r<R$ and compressive for $r>R$. Both stress components are equal to $T(1+\nu)/R$ at the center $r=0$. In the two-dimensional analogue of the problem, in which the uniform shear stress is applied on the surface of a half-space from $x=-a$ to $x=a$, the longitudinal stress σ_x along the surface of the half-space is also singular at $x=\pm a$, being compressive at $x=a$ and tensile at $x=-a$.

7. Reciprocal properties

Once the expression for the radial displacement due to vertical ring load is derived, the expression for the vertical displacement due to radial ring load can be deduced directly by applying the Betti reciprocal theorem. Indeed, from Fig. 16(a), one can write

$$2r\pi Vu_z^{T,R}(r)=2R\pi Tu_r^{V,r}(R). \tag{85}$$

The superscripts (V,r) in $u_r^{V,r}$ designate that the load V is applied at the radius r, and likewise for the superscripts (T,R) in $u_z^{T,R}$. Since, from (19),

$$u_r^{V,r}(R)=\frac{V(1-2\nu)}{2G}\begin{cases}\frac{r}{R}, & r<R,\\ 0, & r>R,\end{cases} \tag{86}$$

(85) gives

$$u_z^{T,R}(r)=\frac{T(1-2\nu)}{2G}\begin{cases}1, & r<R,\\ 0, & r>R.\end{cases} \tag{87}$$

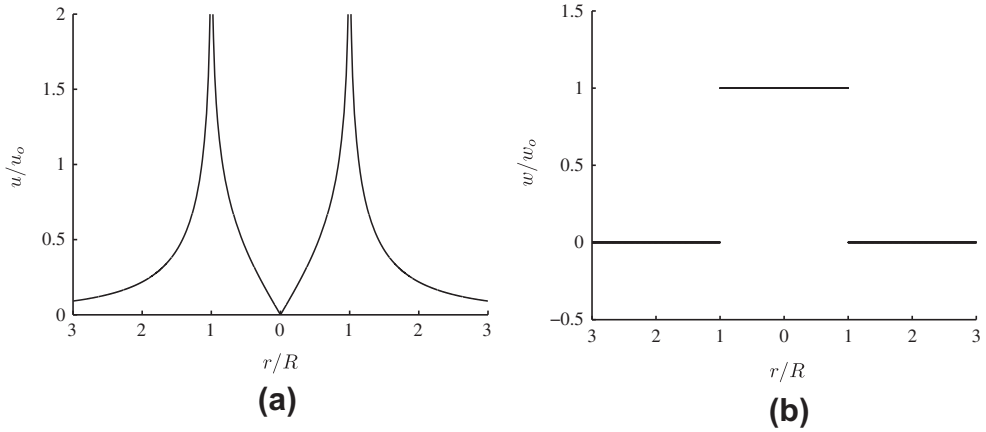

Fig. 15. (a) The radial displacement $u=u_r(r)$ due to radial line load T applied along the circle of radius R, normalized by $u_0=2T(1-\nu)/(\pi G)$, as determined from (76). (b) The corresponding vertical displacement $w=u_z(r)$, normalized by $w_0=T(1-2\nu)/(2G)$, as determined from (68).

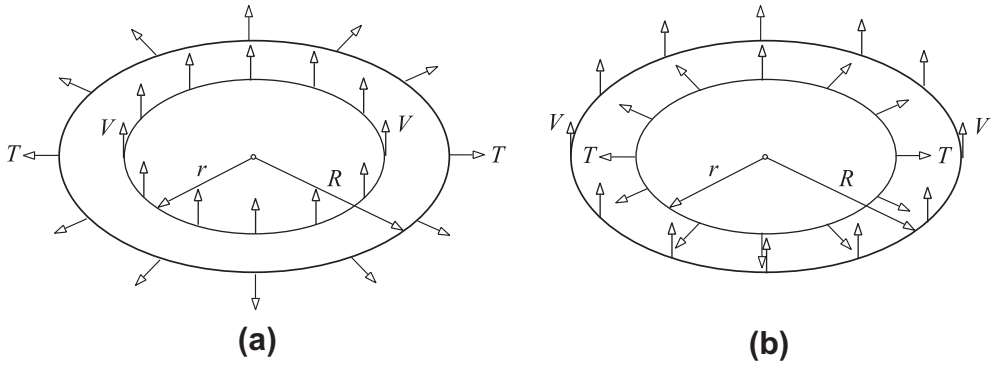

Fig. 16. (a) The surface of a half-space under the vertical ring load along the circle of radius r and the tangential (radial) ring load along the circle of radius R. (b) The vertical ring load applied along the circle of radius R, and the tangential ring load applied along the circle of radius r.

Similarly, once the expression for the vertical displacement due to radial ring load is derived, the expression for the radial displacement due to vertical ring load can be deduced directly by applying the Betti reciprocal theorem. Indeed, from Fig. 16(b), we can write

$$2r\pi T u_r^{V,R}(r) = 2R\pi V u_z^{T,r}(R). \tag{88}$$

Since, from (68),

$$u_z^{T,r}(R) = \frac{T(1-2\nu)}{2G}\begin{cases} 0, & r < R, \\ 1, & r > R, \end{cases} \tag{89}$$

(88) gives

$$u_z^{V,R}(r) = \frac{V(1-2\nu)}{2G}\begin{cases} 0, & r < R, \\ \frac{R}{r}, & r > R. \end{cases} \tag{90}$$

8. Uniformly distributed radial shear stress within a circular area

Consider the problem of a uniform radial shear stress τ applied within a circular area of radius R, as depicted in Fig. 7(b). Upon the integration of the displacement expressions due to the ring load (68), with $T = \tau \mathrm{d}\rho$, we obtain

$$u_z = \frac{\tau(1-2\nu)}{2G}\begin{cases} R - r, & r \leqslant R, \\ 0, & r \geqslant R. \end{cases} \tag{91}$$

The plot of $w = u_z(r)$ is shown in Fig. 17(b). The vertical displacement of the center point ($r = 0$) is $w_0 = \tau R(1-2\nu)/(2G)$.

The derivation of the expression for the radial displacement u_r is more tedious. For $r \leqslant R$, we have from (76),

$$u_r = \frac{2\tau(1-\nu)}{\pi G}\left\{\int_0^r \left[K\left(\frac{\rho}{r}\right) - E\left(\frac{\rho}{r}\right)\right]\mathrm{d}\rho + \int_r^R \frac{\rho}{r}\left[K\left(\frac{r}{\rho}\right) - E\left(\frac{r}{\rho}\right)\right]\mathrm{d}\rho\right\}. \tag{92}$$

The first integral on the right-hand side of (92) can be evaluated easily,

$$\int_0^r \left[K\left(\frac{\rho}{r}\right) - E\left(\frac{\rho}{r}\right)\right]\mathrm{d}\rho = r\int_0^1 [K(k) - E(k)]\mathrm{d}k = r\left(C - \frac{1}{2}\right), \quad k = \frac{\rho}{r} \leqslant 1, \tag{93}$$

where $C = 0.915965\ldots$ is Catalan's constant.

The evaluation of the second integral on the right-hand side of (92) is more involved. First, we note that

$$J = \int_r^R \frac{\rho}{r}\left[K\left(\frac{r}{\rho}\right) - E\left(\frac{r}{\rho}\right)\right]\mathrm{d}\rho = \frac{1}{2}r\int_1^{r/R} [K(k) - E(k)]\mathrm{d}\left(\frac{1}{k^2}\right), \quad k = \frac{r}{\rho} \leqslant 1 \tag{94}$$

and the integration by parts gives

$$J = \frac{1}{2}r\left\{\frac{1}{k^2}[K(k) - E(k)]\right\}_1^{r/R} - \frac{1}{2}r\int_1^{r/R} \frac{1}{k^2}\frac{\mathrm{d}}{\mathrm{d}k}[K(k) - E(k)]\mathrm{d}k. \tag{95}$$

Incorporating (50), the integral on the right-hand side of (95) becomes

$$\int_1^{r/R} \frac{1}{k^2}\frac{\mathrm{d}}{\mathrm{d}k}[K(k) - E(k)]\mathrm{d}k = \int_1^{r/R} \frac{E(k)}{k}\mathrm{d}k + \int_1^{r/R} \frac{kE(k)}{1-k^2}\mathrm{d}k, \tag{96}$$

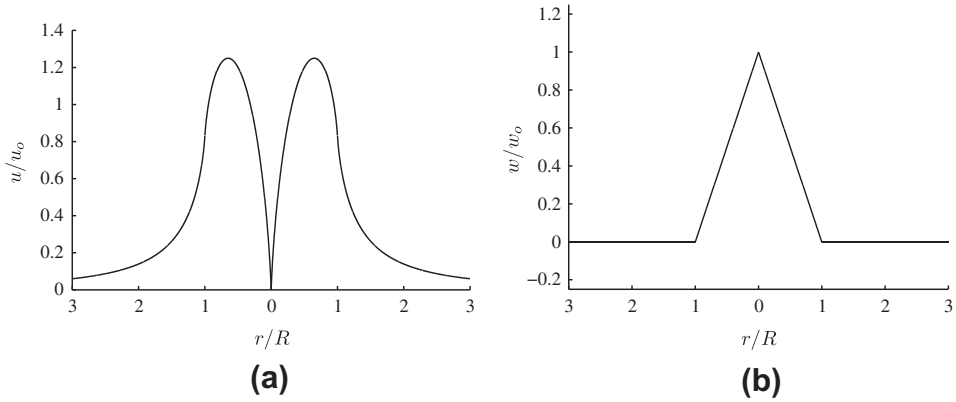

Fig. 17. (a) The radial displacement $u = u_r(r)$ due to uniform radial shear τ applied within the circle of radius R, normalized by $u_0 = \tau R(1-\nu)/(\pi G)$, as determined from (99) and (101). (b) The corresponding vertical displacement $w = u_z(r)$, normalized by $w_0 = \tau R(1-2\nu)/(2G)$, as determined from (91).

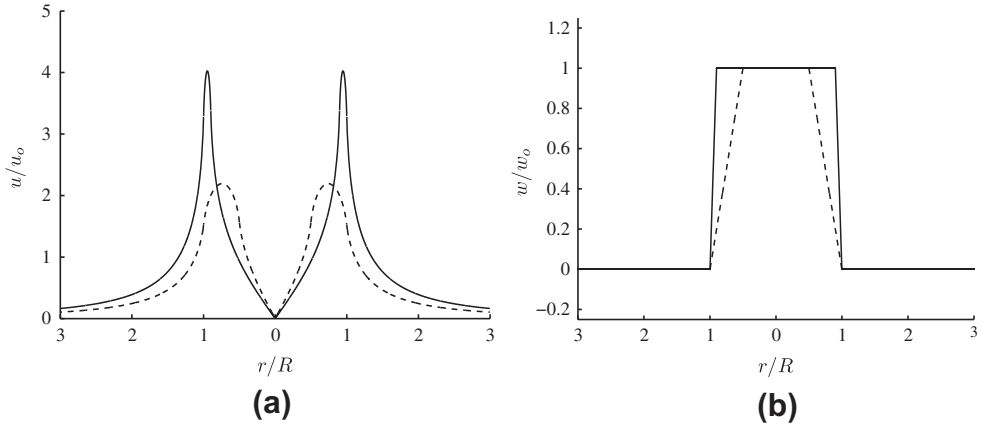

Fig. 18. (a) The radial displacement $u = u_r(r)$ for the loading shown in Fig. 10b. The solid curve is for $R_0 = 0.9R$, and the dotted for $R_0 = 0.5R$. The normalizing displacement factor is $u_0 = (1-\nu)\tau(R-R_0)/(\pi G)$. (b) The corresponding vertical displacement $w = u_z(r)$. The normalizing displacement factor is $w_0 = (1-2\nu)\tau(R-R_0)/(2G)$.

i.e.,

$$\int_1^{r/R} \frac{1}{k^2}\frac{\mathrm{d}}{\mathrm{d}k}[K(k)-E(k)]\mathrm{d}k = \int_1^{r/R} \frac{E(k)}{k}\mathrm{d}k + [K(k)-E(k)]_1^{r/R} \tag{97}$$

and, therefore, (95) becomes

$$J = \frac{1}{2}r\left\{\left(\frac{R^2}{r^2}-1\right)\left[K\left(\frac{r}{R}\right)-E\left(\frac{r}{R}\right)\right] - \int_1^{r/R}\frac{E(k)}{k}\mathrm{d}k\right\}. \tag{98}$$

Finally, by substituting (93) and (98) into (92), the radial displacement is

$$u_r = \frac{\tau(1-\nu)}{\pi G}r\left\{2C-1+\left(\frac{R^2}{r^2}-1\right)\left[K\left(\frac{r}{R}\right)-E\left(\frac{r}{R}\right)\right] + \int_{r/R}^1 \frac{E(k)}{k}\mathrm{d}k\right\},$$
$$r \leqslant R. \tag{99}$$

The evaluation of the remaining integral in (99) can be done numerically.

For $r \geqslant R$, the radial displacement is

$$u_r = \frac{2\tau(1-\nu)}{\pi G}\int_0^R \left[K\left(\frac{\rho}{r}\right)-E\left(\frac{\rho}{r}\right)\right]\mathrm{d}\rho, \tag{100}$$

i.e., by introducing $k = \rho/r$,

$$u_r = \frac{2\tau(1-\nu)}{\pi G}r\int_0^{R/r}[K(k)-E(k)]\mathrm{d}k, \quad r \geqslant R. \tag{101}$$

The integrals on the right-hand side of (101) can also be evaluated numerically. The plot of $u = u_r(r)$ is shown in Fig. 17(a). The maximum radial displacement is $u_{\max} = 1.2502u_0$ and it occurs at $r = 0.6518R$. The radial displacement at $r = R$ is $u(R) = 0.8319u_0$, where $u_0 = \tau R(1-\nu)/(\pi G)$.

The nonvanishing surface strain components are calculated from (99) and (101) as $\epsilon_\theta = u_r/r$, and $\epsilon_r = \mathrm{d}u_r/\mathrm{d}r$. The surface stress components follow from Hooke's law and their plots are shown in Fig. 9(b). The radial and circumferential stresses are singular at the center $r = 0$ and at the radius $r = R$.

9. Radial shear load over an annular ring

To eliminate the singularity and the discontinuity in the displacement under the concentrated radial ring load, it may be assumed that the radial load is distributed over a small but finite thickness. The vertical displacement along the surface of a half-space due to the loading shown in Fig. 10(b) is readily obtained from (28) by superposing the displacements due to radial shear stress τ within the circle $r \leqslant R$ and the opposite shear stress of the same magnitude within the circle $r \leqslant R_0 < R$. By using (91), this gives

$$u_z = \frac{\tau(1-2\nu)}{2G}\begin{cases} R-R_0, & r \leqslant R_0, \\ R-r, & R_0 \leqslant r \leqslant R, \\ 0, & r \geqslant R. \end{cases} \tag{102}$$

Similarly, by using (99) and (101), the radial displacement is found to be

$$u_r = \frac{\tau(1-\nu)r}{\pi G}U_r, \tag{103}$$

where

$$U_r = \begin{cases} \left(\frac{R^2}{r^2}-1\right)\left[K\left(\frac{r}{R}\right)-E\left(\frac{r}{R}\right)\right] - \left(\frac{R_0^2}{r^2}-1\right)\left[K\left(\frac{r}{R_0}\right)-E\left(\frac{r}{R_0}\right)\right] \\ \quad + \int_{r/R}^{r/R_0}\frac{E(k)}{k}\mathrm{d}k, \qquad r \leqslant R_0, \\ 2C-1+\left(\frac{R^2}{r^2}-1\right)\left[K\left(\frac{r}{R}\right)-E\left(\frac{r}{R}\right)\right] + \int_{r/R}^1 \frac{E(k)}{k}\mathrm{d}k \\ \quad -2\int_0^{R_0/r}[K(k)-E(k)]\mathrm{d}k, \qquad R_0 \leqslant r \leqslant R, \\ \int_{R_0/r}^{R/r}[K(k)-E(k)]\mathrm{d}k, \qquad r \geqslant R. \end{cases}$$

The normalized plots of u_r and u_z are shown in Fig. 18. When compared with the displacements due to the radial line load T, shown in Fig. 15, it is seen that the singularity in the radial displacement and the discontinuity in the vertical displacement under the load have both been eliminated, with the resulting degree of smoothness dependent on the ratio R_0/R.

The nonvanishing surface strain components are calculated from (103) as $\epsilon_\theta = u_r/r$ and $\epsilon_r = \mathrm{d}u_r/\mathrm{d}r$. The surface stress components follow from Hooke's law and are shown in Fig. 12(b). Both stress components are singular at $r = R_0$ and $r = R$. They are both finite and equal to $\tau(1+\nu)\ln(R/R_0)$ at the center $r = 0$. The stress singularities would be eliminated if the applied shear stress τ has gradually rather than abruptly decreased to zero at the boundaries of the loading annulus.

10. Conclusion

We have presented in this paper an analysis of the displacement and stress singularities and discontinuities under various types of circular loads applied to the surface of a half-space. This was accomplished without deriving or using the solutions of the entire boundary value problems, but rather by using only the expressions for the displacement components within the surface of a half-space. These are readily obtained by integrating the expressions

for the surface displacements of the well-known Boussinesq and Cerruti concentrated force problems. Two different representations of the expression for the vertical displacement due to vertical ring load are derived, (16) and (32), and two for the radial displacement due to the radial ring load, (65) and (76). In each case, the derived new representation of the displacement expression is more convenient for the subsequent derivation of the expressions for the displacements due to distributed surface loads. The presented method is used to reproduce the surface stress and displacement expressions of Love's problem, (41), (42) and (47), and to derive a novel solution for the surface displacements and stresses due to uniformly distributed radial shear stress within a circular area, given by (91), (99), (101), and Hooke's law. The displacement and stress expressions are also derived for the distributed normal and shear stresses applied within an annular circular region. In the former case, these are given by (53), (54), (57), and in the latter by (102), (103), and Hooke's law.

For the vertical line load V, the elasticity solution predicts not only the singular (infinite) vertical displacement under the line load, but also a discontinuous radial displacement under that load (Fig. 5). The radial and circumferential stresses are finite but discontinuous under the load, being equal to zero for $r < R$ (Fig. 6(a)). For the radial line load T, the radial displacement is singular under the load, while the vertical displacement is discontinuous (Fig. 15). The corresponding stresses are singular and discontinuous under the load, both being equal to $T(1+\nu)/R$ at the center (Fig. 6(b)). In Love's problem of uniform normal stress applied within a circular area, both displacement components are continuous (Fig. 8), but the radial and circumferential stress components are discontinuous below the boundary of the load (Fig. 9(a)). Both stress components are equal to $p(1+2\nu)/2$ for $r < R$. In the case of a uniform normal stress applied within an annular region, the stresses are discontinuous below both boundaries of the applied load, and equal to zero for $r < R_0$ (Fig. 12(a)). In the problem of uniform radial shear stress applied within a circular area, the displacements are finite and continuous everywhere (Fig. 17), but the radial and circumferential stresses are singular at the center and along the boundary of the load (Fig. 9(b)). Finally, if a uniform radial shear stress is applied within an annular region, the radial and circumferential stress components are singular along both boundaries, but are finite and equal to $\tau(1+\nu)\ln(R/R_0)$ at the center (Fig. 12(b)).

Acknowledgments

This research was supported by the Montenegrin Academy of Sciences and Arts. Discussions with Professor Frank E. Talke and the reviewers comments and suggestions are also gratefully acknowledged.

References

Carré, A., Gastel, J.-C., Shanahan, M.E.R., 1996. Viscoelastic effects in spreading of liquids. Nature 379, 432–434.
Das, S., Marchand, A., Andreotti, B., Snoeijer, J.H., 2011. Elastic deformation due to tangential capillary forces. Phys. Fluids 23, 072006-1–072006-11.
Fortes, M.A., 1984. Deformation of solid-surfaces due to capillary forces. J. Colloid Interf. Sci. 100, 17–26.
de Gennes, P.G., 1985. Wetting: statics and dynamics. Rev. Mod. Phys. 57, 827–863.
Gradshteyn, I.S., Ruzhik, I.W., 1965. Tables of Integrals, Sums and Products. Academic Press, New York.
Jerison, E.R., Xu, Y., Wilen, L.A., Dufresne, E.R., 2011. Deformation of an elastic substrate by a three-phase contact line. Phys. Rev. Lett. 106, 186103-1–186103-4.
Johnson, K.L., 1985. Contact Mechanics. Cambridge University Press, New York.
Kern, R., Muller, P., 1992. Deformation of an elastic thin solid induced by a liquid droplet. Surf. Sci. 264, 467–494.
Lester, G.R., 1961. Contact angles of liquids at deformable solid surfaces. J. Colloid Sci. 16, 315–326.
Liu, J.L., Nie, Z.X., Jiang, W.G., 2009. Deformation field of the soft substrate induced by capillary force. Physica B 404, 1195–1199.
Love, A.E.H., 1929. The stress produced in a semi-infinite solid by pressure on part of the boundary. Phil. Trans. R. Soc. Lond. A 228, 377–420.
Lubarda, V.A., 2012. Mechanics of a liquid drop deposited on a solid substrate. Soft Mat. 8, 10288–10297.
Lubarda, V.A., Talke, K.A., 2011. An analysis of the equilibrium droplet shape based on an ellipsoidal droplet model. Langmuir 27, 10705–10713.
Marchand, A., Das, S., Snoeijer, J.H., Andreotti, B., 2012. Capillary pressure and contact line force on a soft solid. Phys. Rev. Lett. 108, 094301-1–094301-5.
Olives, J., 2010. Surface thermodynamics, surface stress, equations at surfaces and triple lines for deformable bodies. J. Phys.: Condens. Mat. 22, 085005-1–085005-12.
Pericet-Camára, R., Best, A., Butt, H.-J., Bonaccurso, E., 2008. Effect of capillary pressure and surface tension on the deformation of elastic surfaces by sessile liquid microdrops: an experimental investigation. Langmuir 24, 10565–10568.
Roman, B., Bico, J., 2010. Elasto-capillarity: deforming an elastic structure with a liquid droplet. J. Phys.: Condens. Mat. 22, 493101-1–493101-16.
Rusanov, A.I., 1975. Theory of the wetting of elastically deformed bodies. 1. Deformation with a finite contact angle. Colloid J. USSR 37, 614–622.
Shanahan, M.E.R., 1988. The spreading dynamics of a liquid-drop on a viscoelastic solid. J. Phys. D: Appl. Phys. 21, 981–985.
Sneddon, I.N., 1951. Fourier Transforms. McGraw-Hill, New York.
Srolovitz, D.J., Davis, S.H., 2001. Do stresses modify wetting angles? Acta Mater. 49, 1005–1007.
Style, R.W., Dufresne, E.R., 2012. Static wetting on deformable substrates, from liquids to soft solids. Soft Mat. 8, 3177–3184.
Terezawa, K., 1916. On the elastic equilibrium of a semi-infinite solid. J. Coll. Sci. Imp. Univ. Tokyo 37, 16–31 (Article 7).
Timoshenko, S.P., Goodier, J.N., 1970. Theory of Elasticity, third ed. McGraw-Hill, New York.
Yu, Y.-S., Zhao, Y.-P., 2009. Elastic deformation of soft membrane with finite thickness induced by a sessile liquid droplet. J. Colloid Interf. Sci. 339, 489–494.